Scientific Research Publishing

Advances in Materials Physics and Chemistry, 2025, 15(1), 1-21
https://www.scirp.org/journal/ampc
ISSN Online: 2162-5328
ISSN Print: 2162-531X

Chemical Compatibility and Physical Coupling between Allophane and Asphalt

Edward Henry Jiménez Calderón[1*], Ana Emperatriz Paucar Tipantuña[2], Paulina Fernanda Herrera Mullo[2], Washington Ruiz López[1], José Eduardo Bermúdez Portero[1], Margarita Verónica Flor Granda[2,3]

[1]Faculty of Chemical Engineering, Central University of Ecuador, Quito, Ecuador
[2]General Directorate of Postgraduate Studies, Central University of Ecuador, Quito, Ecuador
[3]Civil Engineering and Applied Sciences, Central University of Ecuador, Quito, Ecuador
Email: *ehjimenez@uce.edu.ec

How to cite this paper: Calderón, E.H.J., Tipantuña, A.E.P., Mullo, P.F.H., López, W.R., Portero, J.E.B. and Granda, M.V.F. (2025) Chemical Compatibility and Physical Coupling between Allophane and Asphalt. *Advances in Materials Physics and Chemistry*, **15**, 1-21.
https://doi.org/10.4236/ampc.2025.151001

Received: December 3, 2024
Accepted: January 28, 2025
Published: January 31, 2025

Abstract

Motivated by the promising results of previous research, this study evaluated the feasibility of using Allophane, an Ecuadorian nano-clay, as an additive to improve the mechanical properties of asphalt mixtures. The road construction industry has constantly sought to enhance the performance of asphalt pavements, which are affected by issues such as cracking, deformation, and oxidation. These challenges have driven this research to include nanomaterials to extend the lifespan of road infrastructure and reduce maintenance costs. For this purpose, physical and chemical characterization tests were conducted on conventional asphalt (AC-20) and asphalt modified with different percentages of Allophane. These tests included indirect tensile strength, stiffness modulus, and wear loss tests, as well as rheological analyses to determine the viscoelastic behavior of the material. The conclusions indicate that Allophane significantly improves the strength, stiffness, and durability of asphalt, offering a sustainable and high-performance alternative for the construction and maintenance of asphalt pavements. However, it is noted that the performance of Allophane modified asphalt may degrade after prolonged aging. The research highlights the importance of this nanotechnological additive in improving road infrastructure, extending the lifespan of asphalt pavements, and reducing maintenance costs.

Keywords

Indirect Tensile Strength, Stiffness Modulus, Cantabro Wear Loss, Asphalt Mixture, Allophane

1. Introduction

Research on asphalt pavement has significantly advanced in recent decades, driven by the need to improve the durability and performance of road infrastructures. Despite these advances, asphalt pavements face persistent challenges that affect their longevity and efficiency. Among the most common problems are cracking, deformation, and oxidation, caused by a combination of mechanical, environmental, and chemical factors.

Cracking can be induced by fatigue due to repetitive traffic loads, as well as by thermal changes that cause thermal cracking. Deformation, or rutting, results from the accumulation of plastic deformations under sustained loads, especially in high-temperature conditions. Oxidation, on the other hand, degrades the asphalt binder over time, making it more brittle and susceptible to cracking.

The research project arises in response to the need to improve the physicochemical properties of the asphalt mixture used as a binder in concrete. Recent developments in asphalt modification processes offer opportunities to enhance these properties. In particular, studies on nano-clays have shown that they have very special properties due to their nanometric dimensions [1]-[3].

The main objective of this study is to evaluate the commercialization potential of Allophane as an additive for asphalt mixtures. Based on previous research that has demonstrated the interesting physical and chemical properties of Allophane in other fields, it is proposed to explore its application in the asphalt industry, an area not yet commercially explored [4]-[6].

In this context, Allophane, a nano-clay with a high surface area and an amorphous crystallographic structure, has been identified as a potential asphalt modifier. The unique characteristics of Allophane can significantly enhance the mechanical and rheological properties of asphalt, increasing its strength and durability. This study focuses on using Allophane as an additive in asphalt and evaluating its impact on pavement properties [7]-[9].

The main objective of this study is to evaluate the commercialization potential of Allophane as an additive for asphalt mixtures. Based on previous research that has demonstrated the interesting physical and chemical properties of Allophane in other fields, it is proposed to explore its application in the asphalt industry, an area not yet commercially explored [10].

To this end, the aggregate mixture was prepared in accordance with the General Specifications for Road and Bridge Construction MOP-001-F 2002, and briquettes were produced to evaluate the volumetric properties of the mixture [11]-[13].

Physical and chemical characterization tests were conducted on both conventional AC-20 asphalt and asphalt modified with various percentages of Allophane, following the NTE INEN standards. Asphalt mixtures were designed using the Marshall method, establishing design parameters, theoretical optimal asphalt percentage, and mixing and compaction temperatures [14]-[18].

The behavior of hot asphalt mixtures using both conventional and modified asphalt was also evaluated. To determine their performance, indirect tensile

strength tests, stiffness modulus tests, and Cantabrian wear loss tests were conducted.

The molecular dynamics (MD) simulation method was used to investigate the mechanical properties of the asphalt, the interactions between various fractions, and the effects of aging. Molecular simulation is a computational technique that allows the study of system behavior at the atomic and molecular levels. In this study, MD simulations were performed using the SARA software package and the force field with three-dimensional Navier-Stokes equations to model asphalt molecules and their interactions [19]-[23].

To this end, the three-dimensional Navier-Stokes equations were numerically implemented to simulate the behavior of asphalt additives with Allophane at the molecular scale. This allowed for the demonstration of the relationship between the pressure and velocity fields and the concentration of Allophane and asphalt [24]-[29].

By analogy and by definition of incompressible fluids, we know that the Navier-Stokes equations apply to all fluids, whether they are of macroscopic nature, such as in the study of the atomic nucleus, or as a fluid composed of atoms and molecules, as is the case with the mixture of asphalt and Allophane [30]-[34].

The results obtained show that the molecular structure of asphalt aligns with theories of colloidal and Newtonian fluids. Aging weakens the nano-aggregation behavior of asphaltene molecules and reduces the translational mobility of asphalt molecules. The dynamics of asphalt are understood as a colloid, which is explained by the three-dimensional Navier-Stokes equations. Asphalt is a complex compound that includes a diverse and intricate range of hydrocarbons. However, the SARA method allows the study of its structure to understand the strategic variables that guide aging [35] [36].

Finally, fatigue cracking is one of the main variables affecting the durability of asphalt concrete. Understanding the relationship between the self-healing capacity induced by nanotechnological additives and the service life of asphalt materials at the molecular level is fundamental for preventive maintenance and the improvement of asphalt pavement [36].

However, it is important to note that, although preliminary results are encouraging, the performance of nanomaterial-modified asphalts may degrade with prolonged aging. Therefore, it is crucial to continue researching and developing solutions that mitigate these long-term effects to ensure the effectiveness and durability of road infrastructure.

2. Physicochemical Characterization and Molecular Simulation of Asphalt

2.1. Physical and Chemical Characterization of Conventional Asphalt AC-20 and Modified Asphalt

2.1.1. Performance Grade

The performance grade allows us to determine the rheological properties affected

by aging for construction and service life, as well as the parameters of terrain analysis related to critical failures such as rutting, fatigue, and thermal cracking. The Dynamic Shear Rheometer (DSR) from ANTON PAAR, model PHYSICA MCR 301, was used to measure the performance grade value by varying the temperature. The primary temperature ranges (maximum and minimum) for tests at 10 rad/s are based on the specifications of the Ecuadorian technical standard NTE INEN 3030. The procedure for determining the dynamic shear modulus (G*) and the phase angle (δ) is based on the ASTM D7175-15 standard, which defines the shear deformation resistance of the asphalt binder in the viscoelastic region, with a pressure range from 100 Pa to 10 MPa (Table 1(a) and Table 1(b)).

Table 1. (a) Performance grade results; (b) Performance grade results.

(a)

SAMPLE		AC-20 Asphalt			3% Modified AC-20 Asphalt			4% Modified AC-20 Asphalt		
Test Temperature, ˚C	Frequency, Rad/s	Phase Angle δ, ˚	Complex Modulus G*, kPa	G*/sen δ, kPa	Phase Angle δ, ˚	Complex Modulus G*, kPa	G*/sen δ, kPa	Phase Angle δ, ˚	Complex Modulus G*, kPa	G*/sen δ, kPa
46		70.5	13.3	14.1	71.5	16.1	17	70.4	15.8	16.8
52		73.9	6.01	6.25	74.7	7.49	7.76	73.5	7.56	7.88
58	10	77.4	2.75	2.81	77.9	3.44	3.52	76.8	3.56	3.66
64		**80.4**	**1.3**	**1.31**	**80.7**	**1.62**	**1.64**	**79.8**	**1.68**	**1.71**
70		82.8	0.643	0.648	82.9	0.792	0.798	82.3	0.82	0.83

(b)

SAMPLE		5% Modified AC-20 Asphalt			6% Modified AC-20 Asphalt		
Test Temperature, ˚C	Frequency, Rad/s	Phase Angle δ, ˚	Complex Modulus G*, kPa	G*/sen δ, kPa	Phase Angle δ, ˚	Complex Modulus G*, kPa	G*/sen δ, kPa
46		71.5	15.1	15.9	70.9	15	15.9
52		74.6	7.09	7.36	74	7.08	7.37
58	10	77.9	3.29	3.37	77.1	3.31	3.39
64		**80.7**	**1.71**	**1.77**	**80**	**1.56**	**1.58**
70		83.1	0.749	0.755	825	0.758	0.765

2.1.2. Rotating Thin Film Oven (RTFO)

The Rotating Thin Film Oven (RTFO) simulates short-term aging in asphalt cement using 35 grams of the hot sample in a rotating oven, which is then cooled to room temperature for 1 hour. At the end of the test, the residues are obtained for re-characterization using the previously mentioned methods such as the Cleveland open cup flash point, penetration, softening point, penetration index, ductility, performance grade, absolute viscosity, specific gravity, within no more than 72 hours. This procedure is based on ASTM D2872.

2.1.3. Accelerated Aging of Asphalt Binders Using a Pressurized Aging Vessel (PAV)

This method works with the residue obtained from the sample aged in a rotating thin film oven, simulating plant aging influenced by factors affecting the mixture, as indicated by ASTM D6521-19a. The experiment involves heating the sample until it becomes fluid (<150˚C) and then transferring it to the respective vessel, conditioning it for 20 hours. After that, the trays are placed in the oven for 30 minutes, and the process concludes with the execution of the dynamic shear modulus (DSR) test.

2.2. Evaluation of Hot Mix Asphalt

2.2.1. Indirect Tensile Strength (ITS)

The indirect tensile strength test method, described in the UNE-EN 12697-23:2018 standard, is a technique used to determine the indirect tensile strength (ITS) of bituminous mixtures. This method is crucial for assessing the mechanical properties of paving materials and their ability to withstand stresses during their service life.

- Method Principle

The indirect tensile strength test method is based on applying a diametral load to a cylindrical specimen of bituminous mixture until it fractures. The specimen is subjected to a continuous and constant load along its diameter, generating tensile stresses in the horizontal plane and compressive stresses in the vertical plane. The tensile strength is calculated from the maximum load the specimen can withstand before breaking.

- Necessary Equipment

a) Testing Press: A Marshall-type testing press or similar equipment is used, capable of applying loads with a minimum recommended capacity of 28 kN and a constant deformation rate of (50 ± 2) mm/min.

b) Testing Frame with Loading Strips: The frame should be equipped with hardened steel loading strips with a concave surface corresponding to the nominal radius of the specimen.

c) Thermal Conditioning Devices: The specimens must be thermally conditioned, either by a water bath or a controlled air chamber.

- Test Procedure

a) Specimen Preparation: Cylindrical specimens are prepared in the laboratory by compaction or extracted from an existing pavement layer. Before testing, they are stored at a temperature not exceeding 25˚C for a period ranging from 48 hours to 42 days.

b) Thermal Conditioning: The specimens are conditioned to the selected test temperature (usually 10˚C ± 2˚C) by using a water bath or an air chamber.

c) Placement in the Frame: The conditioned specimen is placed in the testing frame, aligned on the lower loading strip to ensure that the load is applied diametrically.

d) Load Application: The compression of the specimen begins, and a continuous

diametral load is applied at a constant rate until the maximum load and the fracture of the specimen are reached. Both the maximum load and the type of fracture are recorded.

- Calculation of Indirect Tensile Strength

The indirect tensile strength (ITS) is calculated using the formula:

$$\mathrm{ITS} = \frac{2000 * P}{\pi * D * H}$$

where:

P is the maximum load applied (N).

D is the diameter of the specimen (mm).

H is the height of the specimen (mm).

An average value is obtained from the results of at least three individual specimens.

To accept the results, the difference between individual indirect tensile strength values must not exceed 17% of the average value. This method is essential for ensuring the quality and durability of bituminous mixtures used in pavements, providing critical information about their ability to withstand stresses and prolong their service life.

2.2.2. Stiffness Modulus

This method is characterized by measuring the axial deformation experienced by the specimen when respective uniform moving or static loads are applied. The universal servo-hydraulic dynamic equipment is used following the procedures of ASTM D7369 and EN12697-26 standards. The height and diameter data of the briquettes are recorded to condition them in the equipment for 24 hours at the working temperature (10, 20, and 40)˚C.

2.2.3. Cantabro Loss by Use

Based on the Spanish standard NLT-352/00, this method involves recording the initial weight of the sample after being submerged for 24 hours at 60˚C, denoted as P1. Subsequently, the value of P2 is obtained after passing the briquette through the drum for 300 revolutions. The wear value is determined by the difference in weights, which should not exceed 40%.

2.2.4. Molecular Dynamics (MD) Method

The molecular dynamics (MD) method was used to investigate the mechanical properties of asphalt, the interactions between various fractions, diffusion behaviors, and the effects of aging. Molecular simulation is a computational technique that allows the study of system behavior at the atomic and molecular levels. In this study, MD simulations were conducted using the SARA software package and the force field with 3D Navier-Stokes equations to model asphalt molecules and their interactions.

The simulations were carried out under the following conditions:

- Temperature: 298 K (25˚C)

- Pressure: 1 atm (101.325 kPa)
- Simulation time: 10 ns (nanoseconds)
- Sample size: 10,000 molecules

Simulations were performed for both unaged and aged asphalt to understand how aging affects the properties of asphalt at the molecular level. Additionally, diffusion properties and the translational mobility of asphalt molecules were evaluated to study the effects of aging on the dynamic behavior of asphalt.

The three-dimensional Navier-Stokes equations are fundamental to understanding the behavior of all fluids. In this context, chemical reactions are deeply connected with fluid dynamics, highlighting the complexity of these systems. Rewriting equation [11] taken from reference [12].

$$P = \frac{1}{1+e^{kt-\mu(x^2+y^2+z^2)^{\frac{1}{2}}}} = \frac{2}{\mu(x^2+y^2+z^2)^{\frac{1}{2}}} \quad \left((x,y,z)\in\mathbb{R}^3, t\geq 0\right) \tag{1}$$

where:

$r = (x^2 + y^2 + z^2)^{1/2}$, attenuation coefficient, μ, [1/m]; growth coefficient, $k = \frac{p_0}{2p_0 v}$, [1/s] and concentration $C = C_0\frac{1-P}{P}$.

Starting from Equation (1) from reference [12], which probabilistically describes the solution of the 3D Navier-Stokes equations, we can find the fundamental values of the model, which is k, the growth or decay constant of the reaction, and μ, the absorption coefficient. Given that, experimentally, through a thermogravimetric analyzer (TGA), we know the variable $P(x, y, z, t)$, which depends on space (x, y, z) and time t, we can write:

$$P(x,y,z,t) = \frac{C_0}{C(x,y,z,t)+C_0} \tag{2}$$

where CCC, representing the concentration of the analyzed asphalt, is its mass and depends on space and time (x, y, z, t). Analogously, using Equation (1), we obtain k, μ and b through two regressions.

$$P = \frac{2}{\mu}\frac{1}{r} \tag{3}$$

$$\ln\left(\frac{1-P}{P}\right) + \frac{2}{P} = kt + b \tag{4}$$

3. Results

3.1. Characterization of Allophane

The following presents the results of the physicochemical characterization of natural Allophane (Table 2).

1) Surface Area Analysis

The determination of specific surface area through nitrogen adsorption capacity is a fundamental technique for characterizing porous materials such as Allophane. The surface area, influenced by factors such as porosity and particle size,

is directly proportional to the adsorption capacity of the material. The results obtained for Allophane, with a surface area exceeding 300 m^2/g, confirm its highly porous nature and its potential for applications in adsorption processes [37].

Additionally, these results align with the values reported in the literature by Kaufhold Stephan for this mineral.

2) Fourier Transform Infrared Spectroscopy (FT-IR)

FT-IR analysis was employed to characterize the molecular structure of Allophane. This technique is based on the absorption of infrared radiation by molecules, producing a characteristic spectrum.

The results showed the presence of absorption bands characteristic of aluminum-rich Allophane, particularly in the regions of 975 - 1020 cm^{-1}, with an intense band centered at 1013.7 cm^{-1} attributed to Si-O-Al stretching vibrations, typical of this clay mineral. The presence of a broad band in the region of 3452 cm^{-1} corresponds to O-H stretching vibrations, indicating the presence of adsorbed water and structural hydroxyl groups. These results confirm the hydrophilic nature of Allophane and its amorphous structure, characterized by a high density of hydroxyl groups.

3) X-Ray Diffraction (XRD)

X-ray diffraction (XRD) is an analytical technique that exploits the interaction of X-rays with crystalline matter. The information obtained from the diffractograms allows for determining the crystalline structure and mineralogical composition of a sample. In the case of Allophane, the diffraction patterns obtained showed a diffuse and low-intensity character, typical of amorphous materials or those with a high degree of structural disorder. Despite these limitations, the presence of the minerals listed in Table 2 was identified, indicating a complex mineralogical composition.

4) Chemisorption

Chemisorption, a technique involving the formation of chemical bonds between the adsorbate and the adsorbent, was employed to characterize the acidic sites of Allophane. Using the temperature-programmed desorption (TPD) technique with ammonia, the distribution of acidic strength of the active sites was determined. The results showed two main desorption peaks at 420 K and 680 K, suggesting the presence of at least two types of acidic sites with different strengths. The determination of the acidic sites was carried out by acid-base titration with ammonia, assuming a stoichiometric relationship of one ammonia molecule per acidic site. The results obtained are summarized in Table 2.

5) X-Ray Fluorescence (XRF)

It is an analytical technique that allows for the non-destructive determination of the elemental composition of a sample. When X-rays strike the sample, the atoms emit characteristic radiation, with energy unique to each element. In this study, wavelength-dispersive XRF (WD-XRF) was used to determine the Si/Al molar ratio in clay minerals. This parameter is fundamental for characterizing the tetrahedral-octahedral structure of these minerals.

Table 2. Physicochemical characterization of allophane.

Test	Result		
1) Surface Area Analysis	**Surface area, m^2/g**		309.09
2) Fourier Transform Infrared Spectroscopy (FT-IR)	**FT-IR infrared spectroscopy, cm^{-1}**	Water Molecule Vibration, OH Groups	3452
		Deformation Caused by H_2O	1639
		Allophane rich in aluminum	1013.7
3) X-Ray Diffraction (XRD)	**Diffraction pattern, % mass percentage**	Quartz, SiO_2	14.2
		Albite, $NaAlSi_3O_8$	----
		Anorthite, Ca ($Al_2Si_2O_8$)	----
		Cristobalite, SiO_2	13.2
		Actinolite, $Ca_{1.73}Na_{0.27}Mg_{1.88}Fe^{2+}_{2.72} + AI_{0.55}Fe^{3+}_{0.32}Mn^{2+}_{0.16}Si_{7.68}O_{22}(OH)_2$	18.6
		N K-Feldspar Group (Sanidine, Microcline, Orthoclase), $KAlSi_3O_8$	----
		Chlorite Group, $Mg_{3.75}Fe^{2+}_{1.25}AI_{1.00}Si_{3.00}O_{10}(OH)_8$	4.5
		Tridymite, SiO_2	----
		Gibbsite, $Al(OH)_3$	49.5
4) Chemisorption	**Active sites**		426
5) X-Ray Fluorescence (XRF)	**elemental composition, mass**	Na_2O	<0.02
		MgO	1.239
		Al_2O_3	29.219
		SiO_2^-	29.732
		P_2O_5	0.056
		TAN_3	<0.05
		K_2O	0.008
		CaO	0.59
		TiO_2	0.919
		Mn_2O_3	0.123
		Fe_2O_3	9.288
		PPC	26.39
	Si/Al ratio		1.02
6) Atomic Force Microscopy (AFM)	**Pore size, nm**		**50**
7) Moisture Content	**Water content in the sample, %**		**47**
8) Apparent Density, g/cm^3			1.9
9) Particle Size Analysis	**Percentage Retained, µm**	>20	0.01
		40	0.16
		60	0.80
		80	1.73
		>80	97.31

6) Atomic Force Microscopy (AFM)

It is a scanning probe microscopy technique that allows for obtaining images of surfaces with nanometric resolution. Using AFM, the surface morphology of Allophane was characterized, obtaining high-resolution images that revealed a maximum pore size of 50 nm. Additionally, the average particle heights were quantified, finding values in the nanometer range. These results confirm the nanometric nature of Allophane and provide valuable information about its surface structure.

7) Moisture Content

The moisture content of the sample was determined using the conventional gravimetric oven-drying method. The obtained value was 47%, which falls within the range of 20% - 50%, as reported by Stephan Kaufhold for similar samples [37].

8) Apparent Density

The apparent density of the Allophane was determined using the pycnometer method, yielding a value of 1.9 g/cm^3. This value is crucial for designing compaction and molding processes for Allophane. This property directly influences the mechanical strength and dimensional stability of materials based on this mineral.

9) Particle Size Analysis

The particle size distribution of the sample was characterized using an image analysis technique based on Stokes' Law. By recording the trajectory of particles in a light beam, a real-time particle size distribution curve was obtained. The results reveal that the sample is primarily composed of particles larger than 80 micrometers.

3.2. Physical and Chemical Characterization of Conventional AC-20 Asphalt and Modified Asphalt

For this purpose, penetration tests, softening point, penetration index, ductility, Cleveland open cup flash point, performance grade, absolute viscosity, and specific gravity tests were conducted according to NTE INEN or ASTM standards, depending on the test, for conventional AC-20 asphalt and asphalt modified with various percentages of Allophane, as shown in **Table 3(a)** and **Table 3(b)**.

In the case of the performance grade (PG) test with the complex modulus, it was performed at various temperatures. However, the results were compared at a maximum temperature of 64˚C, in accordance with the INEN 3030:2017 standard, which means (PG 64, max. 22 min.). "PG" stands for Performance Grade, and the 22-minute period indicates the duration for which the asphalt is expected to maintain certain properties at this maximum temperature, as shown in **Table 1**.

3.3. Tests on Thin Film Oven Residues (RTFO)

This method allowed simulating short-term aging in asphalt cement. It was executed using the residues obtained to recharacterize with the following methods: Cleveland open cup flash point, penetration, softening point, penetration index, ductility, performance grade with dynamic shear modulus, absolute viscosity, and specific gravity. For the absolute viscosity test, it was conducted at a temperature

Table 3. (a) Results of the physical and chemical characterization of conventional and modified asphalt; (b) Results of the physical and chemical characterization of conventional and modified asphalt.

(a)

CHARACTERIZATION OF CONVENTIONAL AND MODIFIED ASPHALT.											
TEST		Unit	Test Standard	AC-20 Asphalt Requirements			Test Results				
				Standard	Min.	Max.	AC-20 Asphalt	3% Modified AC-20 Asphalt	4% Modified AC-20 Asphalt	5% Modified AC-20 Asphalt	6% Modified AC-20 Asphalt
Penetration (25˚C, 100 g, 5 s)		1/10 mm	NTE INEN 917:2013	MOP-001-F:2002	60	70	70	62	62	**60**	66
Softening Point R&B		˚C	ASTM D36	MOP-001-F:2003	48	57	49	49	**51**	**51**	**51**
Penetration Index		---	ASTM D5	MOP-001-F:2004	−1.5	+1.5	−0.64	−0.95	**−0.45**	**−0.54**	−0.71
Ductility (25˚C, 5 cm/min)		cm	NTE INEN 0916	MOP-001-F:2005	100	---	115.8	**77.1**	**75.1**	**70.3**	**56.5**
Flash Point Cleveland Cup		˚C	NTE INEN 0808:2013	MOP-001-F:2006	232	---	272	282	279	**285**	278
Performance Grade	Dynamic Shear Modulus	KPa	ASTM D7175	NTE INEN 3030:2017	1	---	1.6	1.64	1.71	**1.57**	1.58
	Test Temperature at 10 rad/s	˚C			---	---	64	64	64	64	64
Absolute Viscosity (60˚C)		Pa*s	NTE INEN 810 ASTM D2171	NTE INEN 2515:2014	160	240	238	313	278	**276**	360
Absolute Viscosity (25˚C)		g/cm^3	NTE INEN 923 ASTM D70	REPORT			1.01	1.021	1.024	1.024	1.034

(b)

TESTS ON RESIDUES OF THIN FILM OVEN TEST (RTFO)											
TEST		Unit	Test Standard	AC-20 Asphalt Requirements			Test Results				
				Standard	Min.	Max.	AC-20 Asphalt	3% Modified AC-20 Asphalt	4% Modified AC-20 Asphalt	5% Modified AC-20 Asphalt	6% Modified AC-20 Asphalt
Penetration (25˚C, 100 g, 5 s)		% of original	NTE INEN 917: 2013 ASTM D5	MOP-001-F-2006	54*	---	42	41	41	40	40
Softening Point R&B		˚C	ASTM D36	---	---	---	58	58	58	59	59
Penetration Index		---	ASTM D5	---	---	---	0.19	0.15	0.14	0.29	0.30
Ductility (25˚C, 5 cm/min)		cm	NTE INEN 0916: 2013 ASTM D113	MOP-001-F-2006	50	---	25	22	21	16.5	15
Ductility	Dynamic Shear Modulus	KPa	ASTM D7175	NTE INEN 3030:2017	2.2	---	4.91	5.11	4.23	4.91	4.95
	Test Temperature at 10 rad/s	˚C			---	---	64	64	64	64	64
Absolute Viscosity (60˚C)		Pa*s	NTE INEN 810 ASTM D2171	ASTM D3381-92:1999	---	1000	1000	1430	1170	1360	1410
TESTS ON THE RESIDUE OF ACCELERATED AGING OF ASPHALT BINDERS (PAV)											
Performance Grade	Dynamic Shear Modulus	KPa	ASTM D7175	NTE INEN 3030:2017	5000	---	2480	2450	2350	2670	2100
	Test Temperature at 10 rad/s	˚C			---	---	22	22	22	22	22

*54% of original penetration.

of 60˚C, as the NTE INEN 2515:2014 standard classifies semi-solid asphalt cements in Ecuador under this temperature condition. The absolute viscosity results of the AC-20 asphalt are 238 Pa*s, a value that falls within the requirement range of the NTE INEN 2515:2014 standard.

3.4. Accelerated Aging of Asphalt Binders Using the Pressure Aging Vessel (PAV)

For this method, the residue obtained from the sample aged in the rotating oven was used to determine a higher performance grade with a dynamic shear modulus, indicating an asphalt with better mechanical and thermal properties, capable of providing superior performance under adverse conditions and extending the pavement's lifespan.

3.5. Performance Evaluation of Hot Mix Asphalt with Conventional and Modified Asphalt

3.5.1. Indirect Tensile Test

This test evaluates the resistance of the asphalt mixture to tensile forces occurring in the lower fiber of the asphalt mat during operation. It is also an indicator of the cohesion within the mixture, as once the specimen breaks, it is observed whether the aggregates or the cohesion failed. In this case, almost all tested specimens showed intact aggregates, indicating a failure of cohesion.

The mixture modified with 5% Allophane produces greater resistance compared to AC-20 asphalt, as shown in Table 4.

Table 4. Indirect tensile test results.

Sample	N°	Diameter cm	Height cm	Reading	Measurement. kg	Indirect Tensile Strength kg/cm²
AC-20 Asphalt	1	10.22	6.04	249	839	8.5
	2	10.23	6.00	245	825	8.7
	3	10.22	6.02	243	819	8.6
			Average			**8.6**
3% Modified AC-20 Asphalt	1	10.2	5.95	241	812	8.52
	2	10.19	5.58	234	789	8.83
	3	10.3	5.42	226	762	8.69
			Average			**8.68**
4% Modified AC-20 Asphalt	1	10.29	5.63	262	882	9.69
	2	10.24	5.88	244	822	8.69
	3	10.15	5.79	245	825	8.94
			Average			**9.11**
5% Modified AC-20 Asphalt	1	10.30	5.5	271	912	10.3
	2	10.28	5.6	271	912	10.3
	3	10.30	5.7	276	929	10.2
			Average			**10.2**
6% Modified AC-20 Asphalt	1	10.28	5.72	239	805	8.72
	2	10.21	6.59	306	1029	9.74
	3	10.19	5.59	245	825	9.22
			Average			**9.22**

3.5.2. Indirect Tensile Stiffness Modulus Test

The indirect tensile stiffness modulus test enables the characterization of the mixture's behavior when subjected to traffic loads, which induce tensile stresses in the inner fiber of the asphalt pavement. Generally, high stiffness moduli are sought in asphalt mixtures; however, excessively high stiffness moduli values are counterproductive, as they make the mixture more prone to cracking. The asphalt mixture was successfully characterized at different temperatures: (10, 20, and 40)˚C. The stiffness modulus of the asphalt modified with 5% Allophane is higher than the values obtained for AC-20 asphalt, as shown in Table 5.

Table 5. Stiffness modulus results.

T, ˚C	Sample	N˚	Weight, g	Diameter, mm	Height, mm	Density, kg/m³	Stiffness Modulus, MPa			
							Measured		Compacted	
10	AC-20 Asphalt	1	1119	102	63	2172	6984		6942	
		2	1126	102	62	2219	7618	7487	7583	**7448**
		3	1085	102	57	2306	7858		7819	
	3% Modified AC-20 Asphalt	1	1105	102	59.5	2273	8596		8141	
		2	1016	101.9	55.8	2233	7880	8106	8142	**8142**
		3	1051	101.8	57	2275	7842		8142	
	4% Modified AC-20 Asphalt	1	1061	103	56	2266	9073		9086	
		2	1097	102	59	2270	8731	9111	8711	**9101**
		3	1034	103	55	2272	9528		9505	
	5% Modified AC-20 Asphalt	1	1074	103	57	2286	10,099		10,172	
		2	1139	103	59	2288	10,061	9795	10,107	**9835**
		3	1102	103	58	2253	9226		9227	
	6% Modified AC-20 Asphalt	1	1105	103	60	2216	8865		8868	
		2	1082	103	57	2280	85	8774	8557	**8803**
		3	1227	102	66	2278	8947		8995	
20	AC-20 Asphalt	1	1119	102	62	2172	3235		3222	
		2	1126	102	57	2219	3285	3248	3301	**3251**
		3	1085	102	63	2306	3224		3231	
	3% Modified AC-20 Asphalt	1	1105	102	60	2273	3929		3953	
		2	1016	101.8	56	2233	3774	3811	3701	**3813**
		3	1051	102	60	2275	3731		3701	
	4% Modified AC-20 Asphalt	1	1061	103	56	2266	4043		4024	
		2	1097	102	59	2270	4134	4227	4120	**4204**
		3	1034	103	55	2272	4503		4467	
	5% Modified AC-20 Asphalt	1	1074	103	59	2286	4716		4716	
		2	1139	103	58	2288	4401	4561	4570	**4567**
		3	1102	103	57	2253	4567		4414	

Continued

20	6% Modified AC-20 Asphalt	1	1105	103	60	2216	4054	4033	**3917**
		2	1082	103	57	2280	3928	3916 3931	
		3	1227	102	66	2278	3766	3788	
40	AC-20 Asphalt	1	1119	102	63	2172	715	710	**705**
		2	1126	102	62	2219	700	707 701	
		3	1085	102	57	2306	706	705	
	3% Modified AC-20 Asphalt	1	1106	102	60	2273	750	727	**725**
		2	1016	102	56	2233	732	739 728	
		3	1051	101.8	57	2275	734	720	
	4% Modified AC-20 Asphalt	1	1061	103	56	2266	686	684	**736**
		2	1097	102	59	2270	685	738 680	
		3	1034	103	55	2272	844	843	
	5% Modified AC-20 Asphalt	1	1074	103	57	2286	1019	1018	**981**
		2	1139	103	59	2288	951	982 952	
		3	1102	103	58	2253	976	973	
	6% Modified AC-20 Asphalt	1	1105	103	60	2216	904	899	**878**
		2	1082	103	57	2280	851	879 847	
		3	1227	102	66	2278	882	888	

3.5.3. Cantabrian Abrasion Test

The Cantabrian Abrasion test simulates the deterioration conditions of the mixture once it is in service. Thus, the lower the percentage of wear, the better the cohesion between the aggregates and the asphalt, which would prevent the action of vertical traffic loads and atmospheric agents due to wear of the pavement surface. The value of the wear loss result is lower in the case of AC-20 asphalt modified with 5% Allophane, as can be seen in Table 6.

Table 6. Cantabrian abrasion test results.

Sample	N°	Initial Weight, g	Final Weight, g	Percentage of Wear, P
AC-20 Asphalt	1	1085	1059	2.3
	2	1085	1052	3.0
	3	1051	1022	2.8
	Average			**2.7**
3% Modified AC-20 Asphalt	1	115	1089	2.3
	2	1051	1021	2.8
	3	1033	1006	2.5
	Average			**2.6**
4% Modified AC-20 Asphalt	1	1093	1066	2.5
	2	1105.4	1078	2.4

Continued

	3	1074.6	1048	2.5
		Average		**2.5**
5% Modified AC-20 Asphalt	1	1080	1054	2.4
	2	1111	1084	2.4
	3	1043	1017	2.5
		Average		**2.4**
6% Modified AC-20 Asphalt	1	1136	1108	2.4
	2	1016	989	2.7
	3	1072	1045	2,5
		Average		**2.5**

3.6. Dynamics of Asphalt Reaction Using 3D Navier-Stokes Equations

The results obtained using the SARA method, a tool that allows analyzing the structure of modified asphalt to understand the strategic variables influencing its aging, are presented below. Additionally, by applying the three-dimensional Navier-Stokes equations, the dynamics of asphalt additives in the presence of Allophane were simulated, revealing a significant relationship between pressure, velocity, and the concentration of various components. It was determined that the optimal concentration of 5% Allophane improves the properties of the asphalt, suggesting its viability for industrial applications, as shown in Figure 1 and Figure 2.

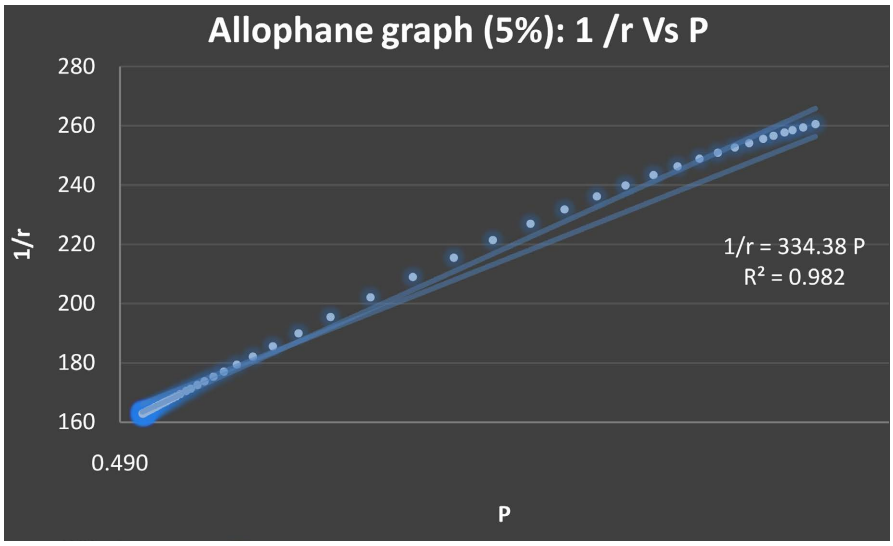

Figure 1. The graph Allophane (5%): $1/r$ vs P indicates the behavior of the probability $P(x, y, z, t)$ or the main solution of the 3D Navier-Stokes equation as a function of the inverse displacement $1/r$. The model's agreement with the experiment is $R^2 = 0.982$. Data from the TGA thermobalance.

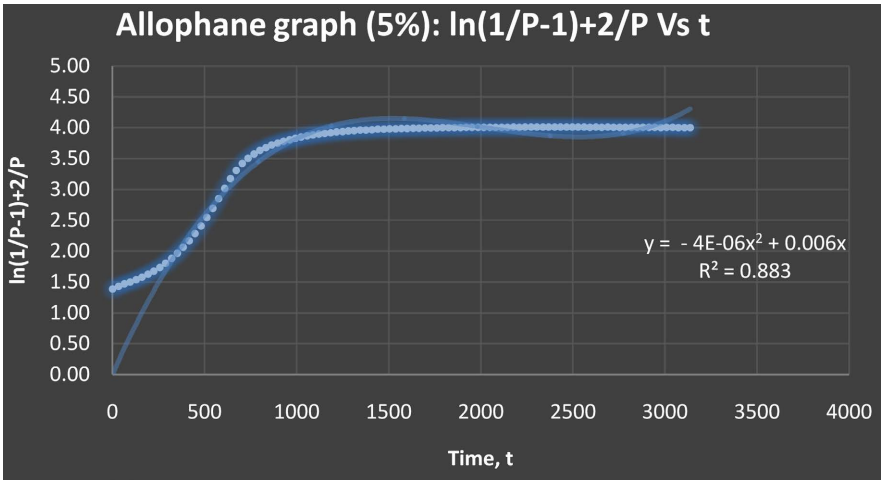

Figure 2. The graph Allophane (5%): ln $(1/P-1)+2/P$ vs t shows the nonlinear behavior of non-Newtonian fluids such as asphalt. This nonlinear evolution is controlled by the 3D Navier-Stokes equations, which allow for the optimal mixture of Allophane and asphalt, with $R^2 = 0.8839$. Data from the TGA thermobalance.

4. Discussion

The evaluation of the properties of asphalt mixtures modified with Allophane, conducted in accordance with INEN standards, has identified the optimal performance of the mixture with 5% Allophane. The dynamic modulus test (NTE INEN 3030:2017) at 64˚C revealed that the mixture with 5% Allophane exhibits the highest performance grade, indicating greater resistance to deformation. Additionally, the complex modulus at 64˚C, which quantifies stiffness, showed a lower value for this mixture, suggesting greater deformability under cyclic loads. The penetration test results, as shown in **Table 3(a)** and **Table 3(b)**, reveal that the mixture with 5% Allophane exhibits the lowest penetration, clearly indicating increased hardness. This directly correlates with the principle that lower penetration values signify a harder asphalt, enhancing its overall durability. Mixtures with 4%, 5%, and 6% Allophane exhibited a softening point of 41˚C, higher than the other mixtures, indicating lower temperature susceptibility. The penetration index for mixtures with 4% and 5% Allophane was −0.45 and −0.54, respectively, suggesting a decrease in hardness with the incorporation of Allophane in these proportions. While the ductility of all mixtures modified with Allophane was below the limit established in NTE INEN 0916, the conventional asphalt showed superior ductility. The Cleveland open cup flash point determines the minimum temperature at which an asphalt emits flammable vapors. According to the test results, the mixture with 5% Allophane has the highest flash point, initiating combustion at 285˚C. In contrast, the conventional asphalt and other modified mixtures show lower flash points, although all comply with the minimum limit of 232˚C established in NTE INEN 0808:2013. The absolute viscosity at 60˚C of the mixture with 5% Allophane exceeded the maximum limit established in NTE INEN 2515:2014, indicating higher viscosity.

The evaluation of asphalt mixtures modified with Allophane, conducted

through indirect tensile tests, stiffness modulus, and Cantabro loss tests (Tables 4-6), has demonstrated superior performance of the mixture with 5% Allophane. This mixture showed greater resistance to fracture, deformation, and wear, as well as greater durability and dimensional stability compared to conventional asphalt and other Allophane proportions. These results suggest that the addition of 5% Allophane optimizes the mechanical properties and durability of asphalt mixtures.

The performance grade for Allophane-modified asphalt presents higher dynamic shear moduli than conventional asphalt, implying increased resistance to shear deformation. Asphalt, when subjected to aging, changes its rheological properties, which is reflected in the dynamic shear modulus results, determining a value above 4 KPa. The dynamic shear modulus of Allophane-modified asphalt always remains higher than that of conventional asphalt. After undergoing an oxidation process (PAV), it can be seen that the dynamic modulus behavior has changed compared to RTFO-aged asphalt, leading to the analysis that 5% Allophane-modified asphalt may become unstable.

Through a self-study, the 3D Navier-Stokes equations (Equations (2)-(4)) have been numerically implemented to simulate the behavior of Allophane asphalt additives at the molecular scale. Figure 1 and Figure 2 show the obtained results, relating the pressure and velocity fields with the concentration of Allophane and asphalt.

5. Conclusions

- The evaluation of the properties of asphalt mixtures modified with Allophane, conducted according to INEN standards, has demonstrated that the mixture with 5% Allophane excels in several key aspects. The results from the dynamic modulus test at 64˚C reveal that this mixture achieves the highest performance level, indicating superior resistance to deformation under cyclic loads. In summary, a higher performance grade directly correlates with greater resistance to deformation, ensuring a more durable and stable asphalt mixture.
- The penetration test showed that the mixture with 5% Allophane has the lowest penetration, indicating higher hardness, a crucial characteristic for applications requiring rigid pavement. Additionally, the mixtures with 4%, 5%, and 6% Allophane demonstrated a softening point above 41˚C, indicating lower temperature susceptibility, thereby improving durability in warm climates.
- The indirect tensile tests, stiffness modulus, and Cantabro wear loss tests revealed that the mixture with 5% Allophane outperforms other mixtures in terms of fracture resistance, deformation, and wear. These findings suggest that adding Allophane at this proportion optimizes the mechanical properties and durability of asphalt mixtures, making it a preferable option compared to other formulations.
- Although the mixture with 5% Allophane has a higher flash point at 285˚C, which is desirable from a safety perspective, the absolute viscosity at 60˚C exceeds the maximum limits established by the NTE INEN 2515:2014 standard.

This suggests that while the mixture has greater thermal stability, its high viscosity could present a challenge in handling and application.

- The performance grade analysis of the Allophane-modified asphalt, subjected to aging processes (RTFO and PAV), shows that the dynamic shear modulus is consistently higher than that of conventional asphalt. However, once aged, the dynamic modulus behavior changes, indicating that the asphalt modified with 5% Allophane could become unstable over time, requiring more detailed analysis for long-term applications.
- The self-taught study that implements the 3D Navier-Stokes equations has enabled the simulation of the molecular-scale behavior of asphalt additives with Allophane. The results obtained show how Allophane concentration affects the pressure and velocity fields in the asphalt, providing a valuable theoretical basis for understanding and predicting the behavior of modified asphalt in practical applications, as evidenced in **Figure 1** and **Figure 2**.

Author Contributions

Conceptualization, PFHM and AEPT; investigation, data curation, analysis, interpretation, and writing: original draft preparation, review, and editing. Investigation, EHJC, WRL, MVFG and JEBP. All authors have read and agreed to the published version of the manuscript.

Funding

This research was funded by the Research Directorate (DI) of the Central University of Ecuador, under the Funded Projects: DI-CONV-2019-017. Physico-chemical Compatibility of Asphalt Additive with Allophane and/or Faujasite.

Acknowledgements

We would like to thank the Research Directorate (DI) of the Central University of Ecuador, as well as the research group of the GIIP process and the Faculty of Chemical Engineering, UCE.

Conflicts of Interest

The authors declare that they have no conflict of interest.

References

[1] Raura, R. (2019) Marshall and Superpave Evaluation of Asphalt Modified with Allophane. Qualification Thesis, Central University of Ecuador.

[2] ASTM International (2019) Standard Test Method for Maximum Theoretical Specific Gravity and Density of Bituminous Mixtures (D2041-D2041M-19). https://www.astm.org/Standards/D2041.htm

[3] ASTM International (2014) Standard Test Method for Sand Equivalent Value of Soils and Fine Aggregates (D2419-14). https://www.astm.org/Standards/D2419

[4] Jiménez, E., Paucar, A. and Herrera, P. (2017) Study of the Catalytic Activity of

Faujasite from Natural Clinker and Pumice Stone. *Physical Chemistry India Journal*, **12**, 1-16.

[5] Jiménez, E., Paucar, A. and Herrera, P. (2019) Technical and Economic Feasibility of the Industrialization of Allophane and Its Use as a Catalyst for the Fluidized Catalytic Cracking Process. Editorial Universitaria, 111-152.

[6] Brito, S., Venegas, E., *et al.* (2019) Sampling Protocol for Soils Derived from Volcanic Ash Rich in Allophane. In: Herrera, P. and Paucar, A., Eds., *Physical Chemistry of Allophane and Their Applications in Crude Oil Refining*, Editorial Universitaria, 57-70.

[7] ASTM International (2019) Standard Test Method for Bulk Density and Unit Weight of Compacted Nonabsorbent Bituminous Mixtures (D2726/D2726M-19). https://www.astm.org/Standards/D2726

[8] Espinosa, T. and Valdivieso, M. (2019) Characterization of Hot Asphalt Mixtures Prepared with Asphalt Nano-Modified with Pure Allophane. Qualification Thesis, Central University of Ecuador.

[9] Kaufhold, S., Dorhmann, Z., Abidin, Z., Henmi, T., Matsue, N., Eichinger, L. and Jahn, R. (2010) Allophane Compared with Other Sorbent Minerals for the Removal of Fluoride from Water with Particular Focus on a Mineable Ecuadorian Allophane. *Applied Clay Science*, **50**, 25-33. https://doi.org/10.1016/j.clay.2010.06.018

[10] Hidalgo, C., Etchevers, J. and Quantin, P. (1991) Imologite in an Andisol from Mexico. *Turrialba*, **41**, 509-514.

[11] ASTM D-287 (2022) Standard Test Method for API Gravity of Crude Petroleum and Petroleum Products (Hydrometer Method). https://store.astm.org/d0287-22.html

[12] Jiménez Calderón, E.H., Paucar Tipantuña, A.E., Herrera Mullo, P.F., Hidalgo Cháfuel, D.A., Ruiz, W., Stahl, U., *et al.* (2020) Natural and Activated Allophane Catalytic Activity Based on the Microactivity Test in ASTM Norm 3907/D3907M-2019. *Applied Sciences*, **10**, Article 3035. https://doi.org/10.3390/app10093035

[13] Filimonova, S., Kaufhold, S., Wagner, F.E., Häusler, W. and Kögel-Knabner, I. (2016) The Role of Allophane Nano-Structure and Fe Oxide Speciation for Hosting Soil Organic Matter in an Allophanic Andosol. *Geochimica et Cosmochimica Acta*, **180**, 284-302. https://doi.org/10.1016/j.gca.2016.02.033

[14] ASTM International (2018) Standard Test Method for Flash and Fire Points by Cleveland Open Cup Tester (D92-18). https://cdn.standards.iteh.ai/samples/100770/b91c6c8ceab44aabbe398086bcc6e546/ASTM-D92-18.pdf

[15] ASTM International (2020) Standard Test Method for Penetration of Bituminous Materials (D5/D5M-20). https://www.astm.org/Standards/D5

[16] ASTM International (2014) Standard Test Method for Softening Point of Bitumen (Ring and Ball Apparatus) (D36/D36M-14). https://www.astm.org/Standards/D36

[17] ASTM International (2017) Standard Test Method for Ductility of Bituminous Materials (D113-17). https://www.astm.org/Standards/D113

[18] McCabe, W., Smith, J.C. and Harriott, P. (2007) Unit Operations in Chemical Engineering. 7th Edition, McGraw Hill, Vol. 1, 875-922.

[19] Wu, M., You, Z., Jin, D., Yin, L. and Xin, K. (2024) Aging Effects on Asphalt Adhesive Properties: Molecular Dynamics Simulation of Chemical Composition and Structural Changes. *Molecular Simulation*, **50**, 836-854. https://doi.org/10.1080/08927022.2024.2359568

[20] Burkert, V.D., Elouadrhiri, L. and Girod, F.X. (2018) The Pressure Distribution inside

the Proton. *Nature*, **557**, 396-399. https://doi.org/10.1038/s41586-018-0060-z

[21] Shanahan, P.E. and Detmold, W. (2019) Pressure Distribution and Shear Forces inside the Proton. *Physical Review Letters*, **122**, Article 072003. https://doi.org/10.1103/physrevlett.122.072003

[22] Qasim, M., Ali, Z., Farooq, U. and Lu, D. (2020) Investigation of Entropy in Two-Dimensional Peristaltic Flow with Temperature Dependent Viscosity, Thermal and Electrical Conductivity. *Entropy*, **22**, Article 200. https://doi.org/10.3390/e22020200

[23] Farooq, U., Afridi, M.I., Qasim, M. and Lu, D.C. (2018) Transpiration and Viscous Dissipation Effects on Entropy Generation in Hybrid Nanofluid Flow over a Nonlinear Radially Stretching Disk. *Entropy*, **20**, Article 668. https://doi.org/10.3390/e20090668

[24] Ji, X. (1997) Deeply Virtual Compton Scattering. *Physical Review D*, **55**, 7114-7125. https://doi.org/10.1103/physrevd.55.7114

[25] Teryaev, O.V. (2016) Gravitational Form Factors and Nucleon Spin Structure. *Frontiers of Physics*, **11**, Article No. 111207. https://doi.org/10.1007/s11467-016-0573-6

[26] Auerbach, N. and Yeverechyahu, A. (1975) Nuclear Viscosity and Widths of Giant Resonances. *Annals of Physics*, **95**, 35-52. https://doi.org/10.1016/0003-4916(75)90042-1

[27] Coppola, G., Capuano, F. and de Luca, L. (2019) Discrete Energy-Conservation Properties in the Numerical Simulation of the Navier-Stokes Equations. *Applied Mechanics Reviews*, **71**, Article 010803. https://doi.org/10.1115/1.4042820

[28] Loveland, W.D., Morrissey, D.J. and Seaborg, G.T. (2005) Modern Nuclear Chemistry. John Wiley & Sons, Inc. https://doi.org/10.1002/0471768626

[29] Pohl, R., Antognini, A., Nez, F., Amaro, F.D., Biraben, F., Cardoso, J.M.R., *et al.* (2010) The Size of the Proton. *Nature*, **466**, 213-216. https://doi.org/10.1038/nature09250

[30] Fefferman, C.L. (2017) Existence and Smoothness of the Navier-Stokes Equation. Clay Mathematics Institute. https://www.claymath.org/wp-content/uploads/2022/06/navierstokes.pdf

[31] Lage, J.L. and Kulish, V.V. (2002) On the Relationship between Fluid Velocity and De Broglie's Wave Function and the Implications to the Navier—Stokes Equation. *International Journal of Fluid Mechanics Research*, **29**, 13 p. https://doi.org/10.1615/interjfluidmechres.v29.i1.30

[32] Caffarelli, L., Kohn, R. and Nirenberg, L. (1982) Partial Regularity of Suitable Weak Solutions of the Navier-Stokes Equations. *Communications on Pure and Applied Mathematics*, **35**, 771-831. https://doi.org/10.1002/cpa.3160350604

[33] Chen, Z., Pei, J., Li, R. and Xiao, F. (2018) Performance Characteristics of Asphalt Materials Based on Molecular Dynamics Simulation—A Review. *Construction and Building Materials*, **189**, 695-710. https://doi.org/10.1016/j.conbuildmat.2018.09.038

[34] Xu, G. and Wang, H. (2017) Molecular Dynamics Study of Oxidative Aging Effect on Asphalt Binder Properties. *Fuel*, **188**, 1-10. https://doi.org/10.1016/j.fuel.2016.10.021

[35] Guo, M., Liang, M., Fu, Y., Sreeram, A. and Bhasin, A. (2021) Average Molecular Structure Models of Unaged Asphalt Binder Fractions. *Materials and Structures*, **54**, Article No. 173. https://doi.org/10.1617/s11527-021-01754-2

[36] Liang, B., Lan, F., Shi, K., Qian, G., Liu, Z. and Zheng, J. (2021) Review on the Self-Healing of Asphalt Materials: Mechanism, Affecting Factors, Assessments and Improvements. *Construction and Building Materials*, **266**, Article 120453.

https://doi.org/10.1016/j.conbuildmat.2020.120453

[37] Kaufhold, S., Kaufhold, A., Jahn, R., Brito, S., Dohrmann, R., Hoffmann, R., *et al.* (2009) A New Massive Deposit of Allophane Raw Material in Ecuador. *Clays and Clay Minerals*, **57**, 72-81. https://doi.org/10.1346/ccmn.2009.0570107